FORSCHUNGSZENTRUM KARLSRUHE
Technik und Umwelt
Wissenschaftliche Berichte
FZKA 6097B

Upgrade of the Monte Carlo Code CORSIKA to Simulate Extensive Air Showers with Energies $> 10^{20}$ eV*

D. Heck and J. Knapp[1†]

Institut für Kernphysik

* Contribution to: Frühjahrstagung DPG, Sektion Teilchenphysik, March 23 - 27 (1998) Freiburg
[1] Universität Karlsruhe, Institut für Experimentelle Kernphysik, Postfach 3640, D-76021 Karlsruhe
† now at: Department of Physics and Astronomy, University of Leeds, Leeds LS2 9JT, United Kingdom

Forschungszentrum Karlsruhe GmbH, Karlsruhe
1998

Abstract

Upgrade of the Monte Carlo Code CORSIKA to Simulate Extensive Air Showers with Energies $> 10^{20}$ eV.

To simulate extensive air showers at the highest observed energies the Monte Carlo program CORSIKA has been upgraded. Some of the uncertainties of the hadronic interaction models are discussed. The effects of the Landau-Pomeranchuk-Migdal effect onto the electromagnetic interactions are demonstrated. Special attention is paid to the reduction of computing time by the so-called *thin sampling* procedure. Various steps of realization are described. The influence of the thin sampling level on the computing time, the particle numbers to be stored, and the statistical uncertainty of observable quantities is shown.

Zusammenfassung

Erweiterung des Monte Carlo Programms CORSIKA zur Simulation von ausgedehnten Luftschauern bei den höchsten Energien $> 10^{20}$ eV.

Um ausgedehnte Luftschauer bei den höchsten beobachteten Energien simulieren zu können, wurde das Monte Carlo Programm CORSIKA erweitert. Einige der Unsicherheiten, die von den hadronischen Wechselwirkungsmodellen herrühren, werden diskutiert. Der Einfluß des Landau-Pomeranchuk-Migdal-Effekts auf die elektromagnetischen Wechselwirkungen wird gezeigt. Besondere Aufmerksamkeit wird der Verminderung der Rechenzeit durch das sogenannte *thin sampling* (Ausdünnen) gewidmet. Die verschiedenen Ausbaustufen der Verwirklichung werden beschrieben. Der Einfluß der Ausdünn-Energieschwelle auf die Rechenzeit, auf die Zahl der zu speichernden Teilchen und auf die statistische Unsicherheit beobachtbarer Größen wird demonstriert.

Contents

1 Introduction

The greatest mysteries of cosmic rays arise at the highest energies ($> 10^{15}\ eV$) where the flux becomes so small that very extended detectors on the Earth surface are needed to collect statistically sufficient events. Such experiments cannot observe the primary cosmic ray directly, rather they look for the reaction products which are formed within the atmosphere - so-called extensive air showers (EAS) - and reach the ground. The reconstruction of parameters like primary energy, direction, and mass is not straight forward and is only possible by comparison with detailed simulations of the EAS development. Special interest is given to cosmic rays at energies $> \ 10^{19}\ eV$ as their existence cannot to be explained consistently with known acceleration mechanisms and large distance traveling through space without interaction with the $3^o\ K$ background radiation. The experimental determination of the precise form of the spectrum at those energies would be a great step towards the understanding of the highest energy particles in the universe.
Some experiments to explore this energy range are now operating or are to be realized in the near future. Such experiments are AGASA [1], HiRes [2], Yakutsk [3], and AUGER [4]. Understanding the experimental data and designing new experiments needs Monte Carlo programs to simulate EAS at the highest energies. These requests pushed the upgrade of the EAS simulation program CORSIKA (**CO**smic **R**ay **SI**mulation for **KA**SCADE) for primary energies $> 10^{20}\ eV$.

2 Features of Hadronic Interaction Models

The most essential ingredient to simulate EAS at the highest energies is a hadronic interaction model which is able to extrapolate from lower energies covered by (man made) accelerators to predict the results of hadronic collisions at higher energies. This extrapolation is subject to considerable uncertainties. Within CORSIKA [5] we have five high energy hadronic interaction models available: DPMJET [6], HDPM [5, 7], QGSJET [8], SIBYLL [9], and VENUS [10]. A comparison of these models is given in Ref. [11, 12, 13] which includes a discussion of their influences onto the development of EAS. Three of these models (DPMJET, QGSJET, and SIBYLL) handle hadronic interactions at the highest energies. Besides other features they predict also the hadronic interaction cross-section which determines the free path between two interactions. The predicted inelastic proton-air cross-sections are shown in Fig. 1. Despite the extrapolation, the cross-section values of the three models do not differ by more than $\approx$ 15 % at the highest energies. Similarly the average transverse momentum which is carried away by the charged secondary particles is predicted in accordance up to $p_{lab} = 10^{19}\ eV$ (corresponding with $E_{cm} \ \approx \ 10^5\ GeV$, see Fig. 8 of Ref. [11]) and the differences between the considered models are moderate. Other extrapolations like the average multiplicity of secondary charged particles emerging from a hadronic collision are affected by a much larger uncertainty

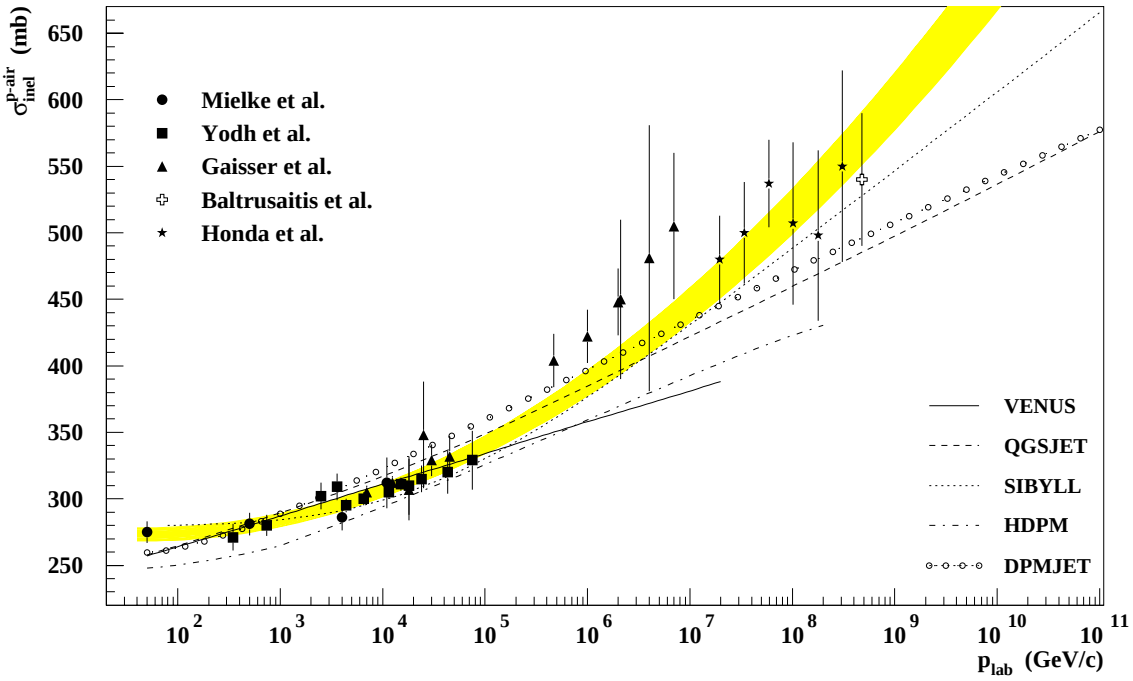

Figure 1: Inelastic p-air cross-sections for hadronic interaction models available in CORSIKA together with experimental values derived from air shower experiments [14, 15, 16, 17, 18]. The shaded band represents a fit to the data below $p_{lab} < 10^5\ GeV$ according to the function $\sigma_{inel}^{p-air} = a \cdot log(p) + b \cdot log^2(p) + c$.

of more than a factor 2.5, as may be deduced from Fig. 5 of Ref. [11].

3 Landau-Pomeranchuk-Migdal Effect

When an ultrarelativistic electron emits a low-energy photon via bremsstrahlung, the longitudinal momentum transfer between electron and the involved target nucleus can be very small. Because of the uncertainty principle this implies a long distance within which the momentum transfer takes place, known as the formation length. If anything happens to one of the two electromagnetic particles while traveling this formation length, the emission can be disrupted. This is known as Landau-Pomeranchuk-Migdal (LPM) effect [19, 20] and is caused predominantly by electron multiple scattering. This effect becomes noticeable for interactions in air (at normal temperature and pressure) at energies above $\approx 10^{16}\ eV$. Similarly in pair production it suppresses predominantly those events in which the energy is shared symmetrically by the e^+e^--pair.

The magnitude of this suppression depends on the product $E_{em} \cdot \rho_{air}$ of the energy of inducing em-particle and of the air density at the interaction point. Consequently for pair production and bremsstrahlung the LPM-effect is most pronounced at high energies and low altitudes. In Figs. 2 and 3 the influences of the LPM-effect are shown

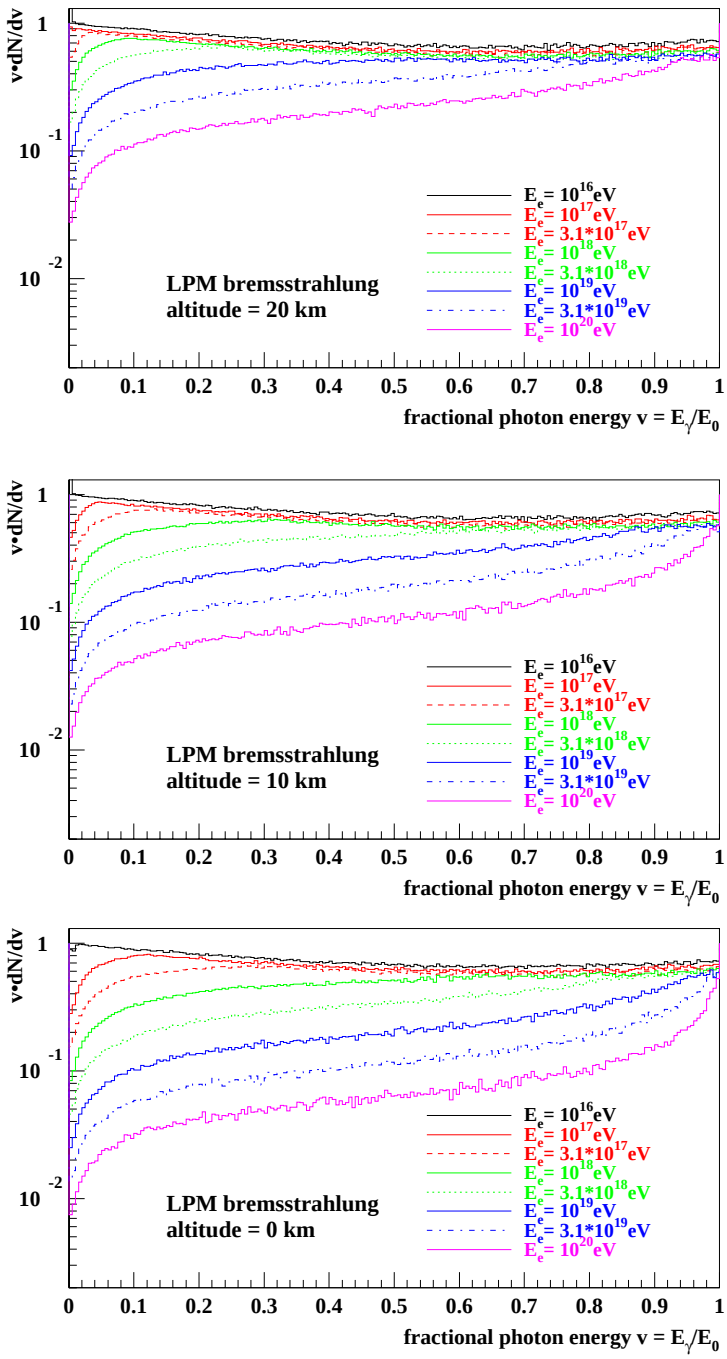

Figure 2: LPM-effect for bremsstrahlung at various altitudes and electron energies. On the ordinate the product of fractional photon energy v times the rate per fractional photon energy dN/dv is given in arbitrary units. For the lowest energies it coincides with the Bethe-Heitler case.

for 3 altitudes and various energies between $E = 10^{16}\ eV$ and $10^{20}\ eV$. These curves have been established with a routine taken from the FORTRAN program AIRES

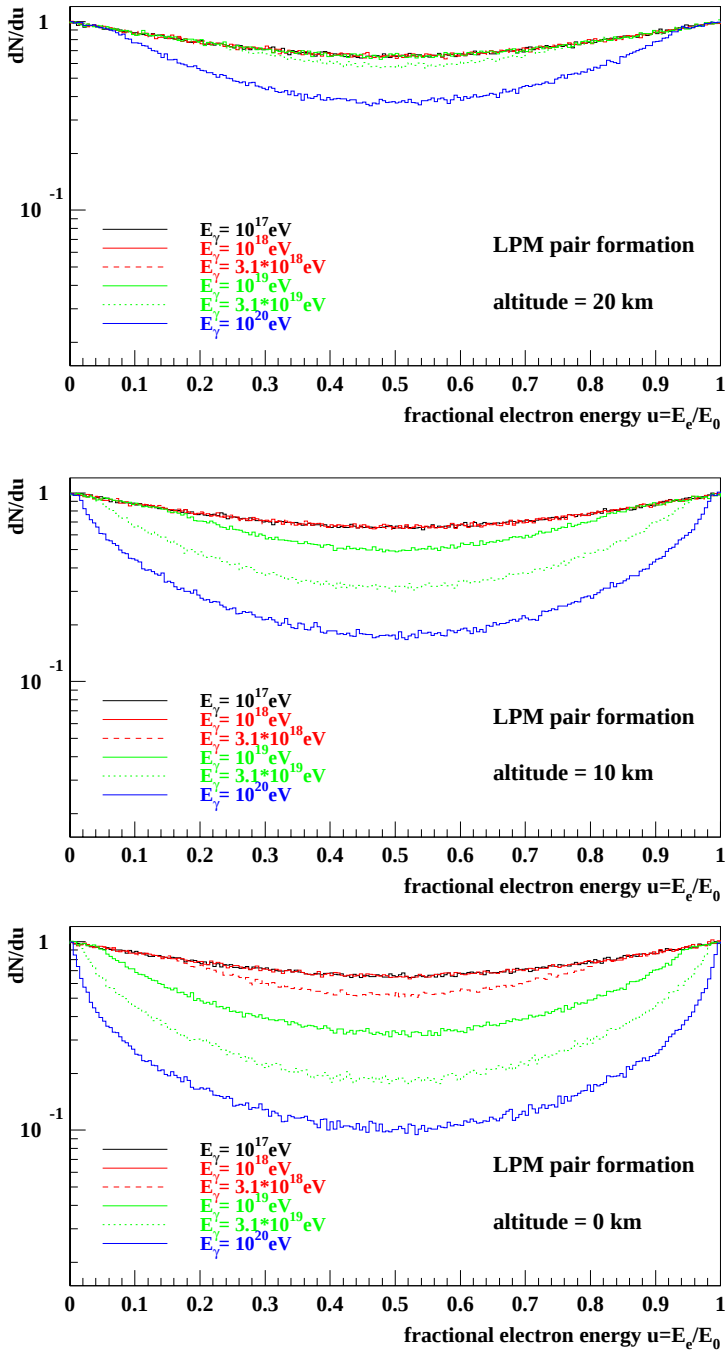

Figure 3: LPM-effect for pair production at various altitudes and gamma-ray energies. On the ordinate the rate per fractional electron energy dN/du is given in arbitrary units. For the lowest energies it coincides with the Bethe-Heitler case.

[21] (which corresponds with the PASCAL program MOCCA [22]) and adapted to CORSIKA.

According to Migdal [20] we use the fractional form to express the energies in the

cross-section formulas following Ref. [23]. The probability per radiation length that an electron with energy E radiates a photon with energy k between $v = k/E$ and $v + dv$ is given by

$$W_b(E,v)dv = \xi(s)\left\{v^2 G(s) + 2\left[1 + (1-v)^2\right]\Phi(s)\right\} dv/3v \quad . \tag{1}$$

Similarly the probability per radiation length that a photon with energy K produces an e^+e^- pair with electron energy p between $u = p/K$ and $u + du$ is expressed as

$$W_p(K,u)du = \xi(\overline{s})\left\{G(\overline{s}) + 2\left[u^2 + (1-u)^2\right]\Phi(\overline{s})\right\} du/3 \quad . \tag{2}$$

The fractional energy of the accompanying positron is $1 - u$. The functions $G(s)$, $\Phi(s)$, and $\xi(s)$ are given by

$$G(s) = 12\pi s^2 - 48 s^3 \sum_{l=0}^{\infty} 1/\left[\left(s + l + \frac{1}{2}\right)^2 + s^2\right] \tag{3}$$

$$\Phi(s) = 6s - 6\pi s^2 + 24 s^3 \sum_{l=0}^{\infty} 1/\left[(s+l)^2 + s^2\right] \tag{4}$$

$$\xi(s) = \begin{cases} 2 & : \quad s \le s_1 \\ 1 + (\ln s/\ln s_1) & : \quad s_1 < s < 1 \\ 1 & : \quad s \ge 1 \end{cases} \tag{5}$$

where $s_1 = \left(Z^{1/3}/190\right)^2$ and Z is the atomic number of the medium. The parameters s and $\overline{s}$ in Eqs. 1 and 2 are given by

$$s^2 = \frac{1}{16}\left(\alpha t_0/\lambda_e\right)\left(mc^2/E\right)\left[\frac{v}{(1-v)\xi(s)}\right] \tag{6}$$

$$\overline{s}^2 = \frac{1}{16}\left(\alpha t_0/\lambda_e\right)\left(mc^2/K\right)\left[\frac{1}{u\ (1-u)\xi(\overline{s})}\right] \tag{7}$$

where α is the fine structure constant, t_0 is the (density dependent) radiation length, λ_e is the Compton wavelength of the electron, and mc^2 is the electron rest mass. Both t_0 and λ_e are measured in cm. The value of the factor $\frac{1}{16}\left(\alpha t_0/\lambda_e\right)$ amounts to $(1.371 \cdot 10^3)^2\ t_0$. For $s > 1$ rsp. $\overline{s} > 1$ which corresponds with a small energy of the primary particle, Eqs. 1 and 2 transform into the familiar Bethe-Heitler cross-sections W_b^{BH} and W_p^{BH} as for this case $G = 1$, $\Phi = 1$, and $\xi = 1$.

In CORSIKA the simulation performs a bremsstrahlung or pair production event always in the ordinary Bethe-Heitler case. Before the secondary particles are stored, the LPM-routine is applied to check, whether the interaction should be discarded. First s^2 rsp. $\overline{s}^2$ is calculated according to Eq. 6 rsp. 7, assuming $\xi = 1$. If $s^2 \ge 1$ rsp. $\overline{s}^2 \ge 1$ then we are in the ordinary low energy case and the parameters of the

secondary particles are completed and stored, the LPM-effect is not effective.

If $s^2 < 1$ rsp. $\overline{s}^2 < 1$ then ξ is determined according Eq. 5 and s rsp. $\overline{s}$ are corrected for the contribution of ξ. In the next step $G(s)$ (Eq. 3) and $\Phi(s)$ (Eq. 4) are calculated using the approximations

$$G(s) = g'/(1+g')$$

with

$$g' = \begin{cases} s^2[14.1 + 2.36/(s+0.1)] & : \quad s < 0.1 \\ s^2[24.0 + 0.0394/(s-0.08)] & : \quad s \geq 0.1 \end{cases}$$

and

$$\Phi(s) = \begin{cases} 6s - 16s^2 & : \quad s < 0.1 \\ 6s + 24s^2\left[\pi/4 - \arctan\left(0.944 + 0.59/s\right)\right] & : \quad s \geq 0.1 \end{cases} \quad .$$

Finally, the fraction of the LPM cross-section according to Eq. 1 or 2 relative to the Bethe-Heitler cross-section (W_b^{LPM}/W_b^{BH} rsp. W_p^{LPM}/W_p^{BH}) is compared with a random number, distributed uniformly between 0 and 1. If the random number exceeds the fraction, the interaction is rejected and the primary particle is propagated further on without interaction.

By the LPM-suppression electromagnetic interactions with extreme asymmetric energy distribution of the secondary particles are favoured. Together with the decreasing electromagnetic cross-sections the net effect onto EAS results in a retarded shower development accompanied by enhanced fluctuations, as demonstrated in Ref. [23]. Our tests with and without LPM-effect revealed, that for γ-induced showers of 10^{20} eV the shower maximum is pushed deeper into the atmosphere by ≈ 100 g/cm^2 slant depth when switching on the LPM-effect.

4 Computing Times without Thin Sampling

The most serious problem in simulations of EAS at the highest energies comes from the nearly linear growth of CPU computing time with primary energy. This growth is shown in Fig. 4 for CORSIKA using EGS full Monte Carlo simulation for electromagnetic particles. Even with today's fast work stations, CPU-times of more than one year per shower for $E_0 > 10^{20}$ eV exceed the limits of feasibility.

A similar problem comes from the huge number of secondaries to be stored when arriving at a detector. The number of 1 million particles for a vertical shower of 10^{15} eV primary energy will explode to about 200 billion particles per shower at 10^{20} eV, which need a storage of ≈ 6 TB.

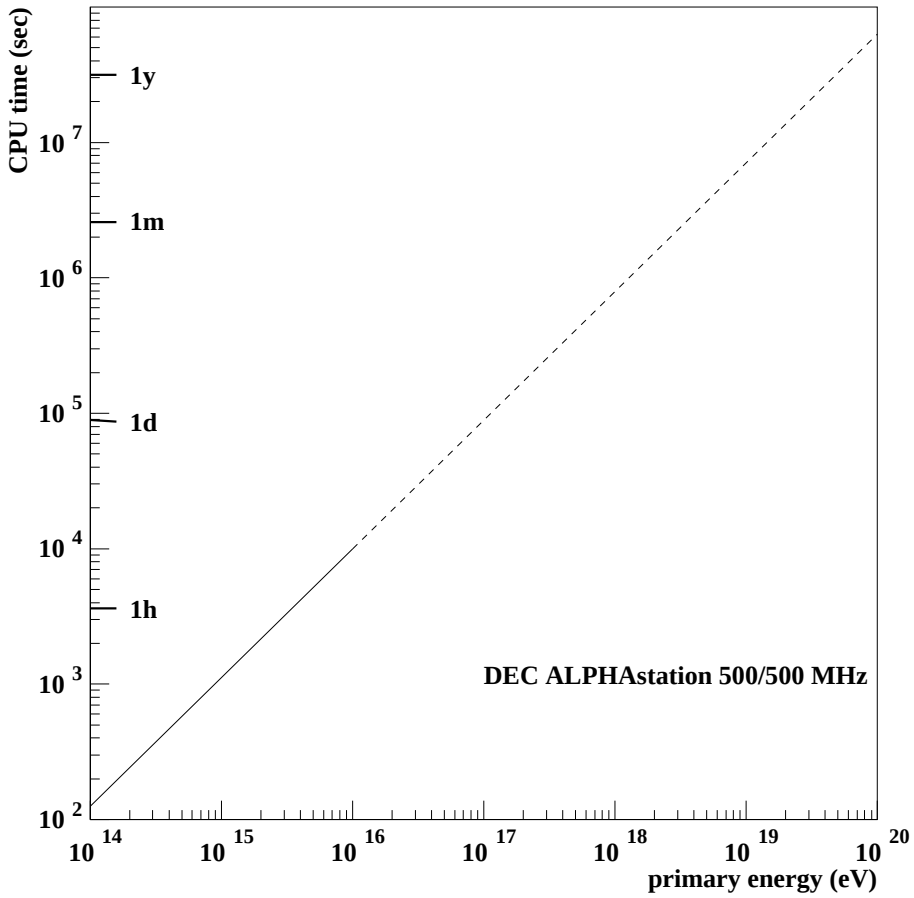

Figure 4: CPU-time as function of the proton primary energy at vertical incidence for full simulation of the electromagnetic subshowers.

5 Stages of Thin Sampling

An elegant way out of the enormous CPU-time consumption has been demonstrated by M. Hillas [22, 24] using the so-called *thin sampling* algorithm. It resembles the *variance reduction* method of Ref. [25].

If an EAS has developed far enough so that very many particles are available, out of the particles emerging from an interaction only one is selected at random to be representative and considered for the further development of the EAS, while the other secondary particles are discarded. The advantage of this procedure is a drastic reduction of CPU-time, as now only few particles have to be followed down to the ground, while the huge bulk of low energy particles not essentially contributing to the gross development of an EAS may be dropped.

The decision at which point of the EAS development the thin sampling should start is given by the thinning level energy E_{thin}, usually expressed by the fraction ε_{thin} of

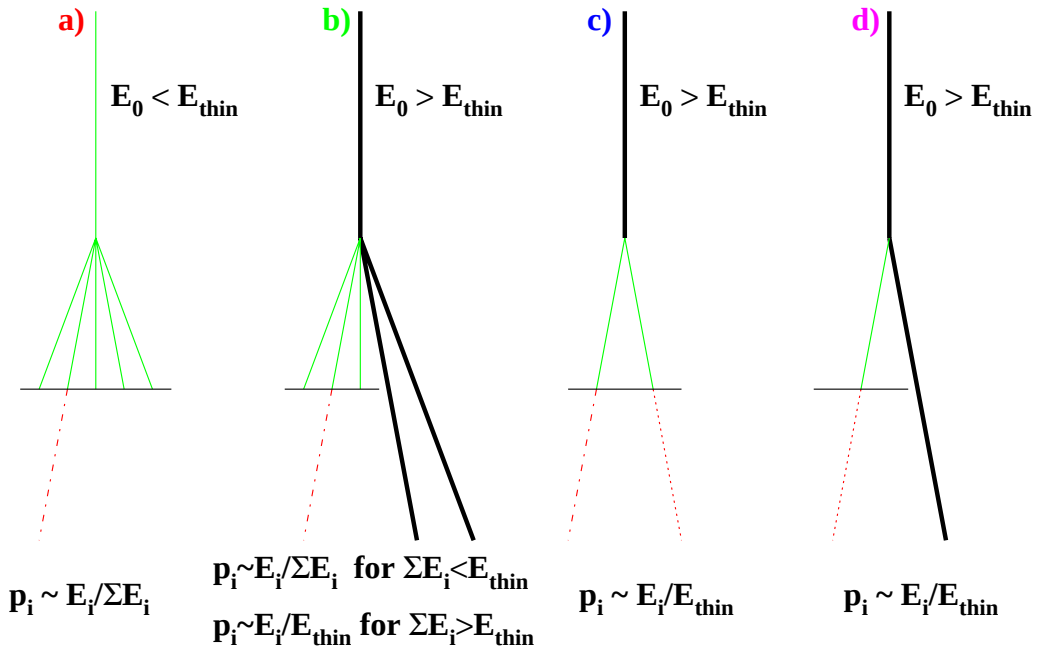

Figure 5: Various development stages of thin sampling in CORSIKA. The horizontal bar below the vertex symbolizes the thin sampling algorithm which passes only the selected particles and discards the others. The summation in case a) and b) runs always over all i secondary particles with $E_i < E_{thin}$. Particles with $E > E_{thin}$ are represented by thick solid lines, particles selected by the thin sampling procedure are given by dashed-dotted and dotted lines.

the primary energy E_0

$$\varepsilon_{thin} = E_{thin}/E_0 \quad .$$

The representative particle is selected at random respecting a survival probability according to its energy fraction of the energy summed over all secondary particles emerging from the interaction under consideration. This is drawn schematically in Fig. 5a). After the selection process the weight of this particle is increased by the weight factor $w_i = 1/p_i$. This first stage a) of development has been used in CORSIKA version 5.20.

Results showed, that still many low energy particles had to be followed. They originate from interactions induced by particles with energy $E > E_{thin}$. Typically such low energy particles with $E_i < E_{thin}$ emerge in the target rapidity range together with high energy particles with energies $E_i > E_{thin}$ in the projectile rapidity range. Depending on the energy sum of those i secondaries with $E_i < E_{thin}$ the survival probability p_i is calculated to

$$\begin{aligned} p_i &= E_i/\textstyle\sum_i E_i \quad \text{for} \quad \textstyle\sum_i E_i < E_{thin} \quad \text{and} \\ p_i &= E_i/E_{thin} \quad \text{for} \quad \textstyle\sum_i E_i \geq E_{thin} \quad . \end{aligned}$$

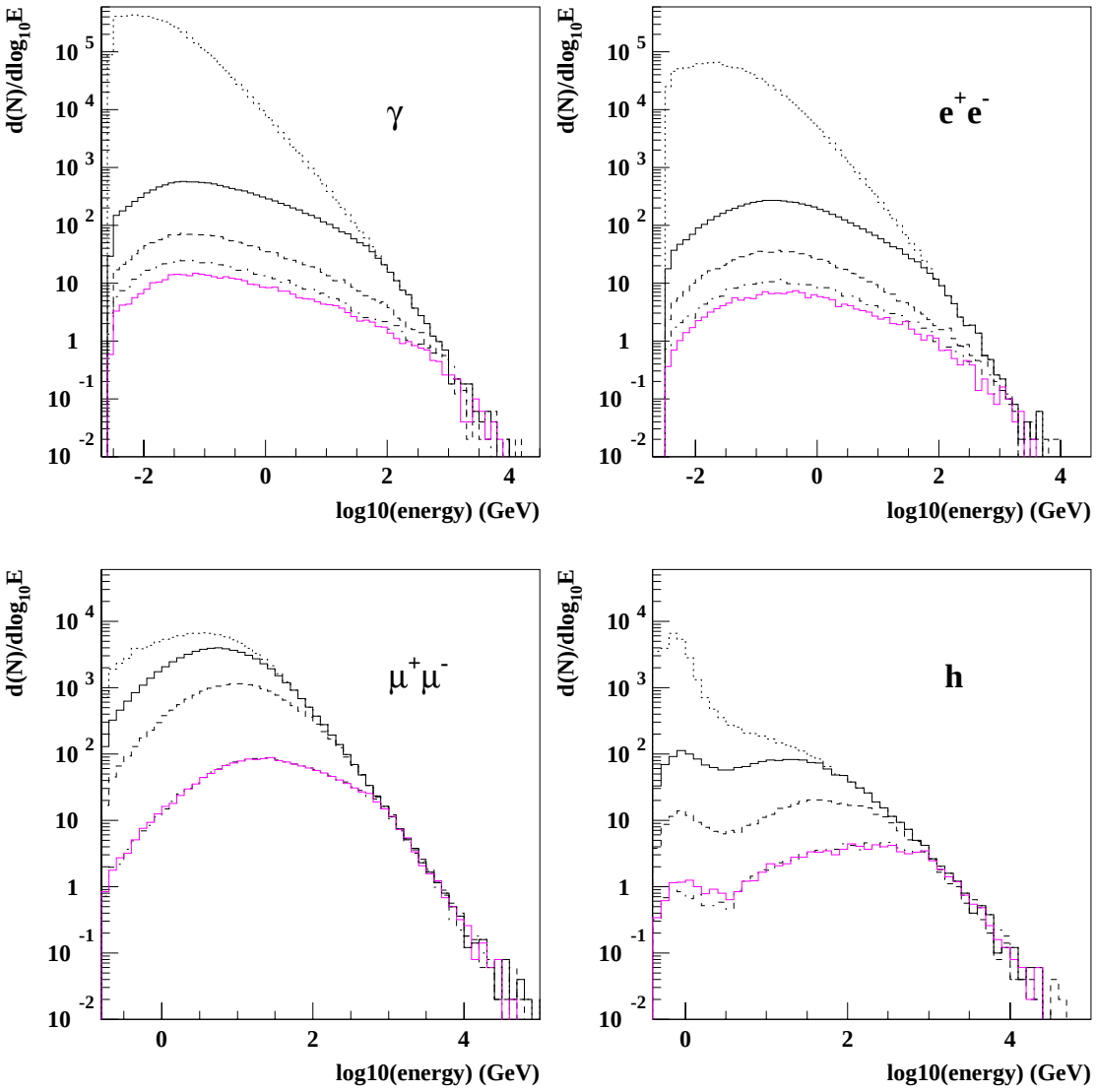

Figure 6: Unweighted energy spectra resulting from various stages of thin sampling for gamma rays (top left), e^+ and e^- (top right), muons (bottom left), and hadrons (bottom right). The gradual reduction of the number of particles reaching the detector level is demonstrated for the cumulative application of the development stages a) (solid line), b) (dashed line), c) (dashed-dotted line), and d) (thin solid line). Proton induced EAS with $E_0 = 10^6\ GeV$ at vertical incidence have been thin sampled below $E_{thin} = 10^3\ GeV$ for this figure using CORSIKA default parameters. The dotted line on top of each plot is without thin sampling.

In the second case the summation over all p_i results in $\sum p_i > 1$ indicating that eventually more than one secondary is retained for further treatment. This case is represented by Fig. 5b).

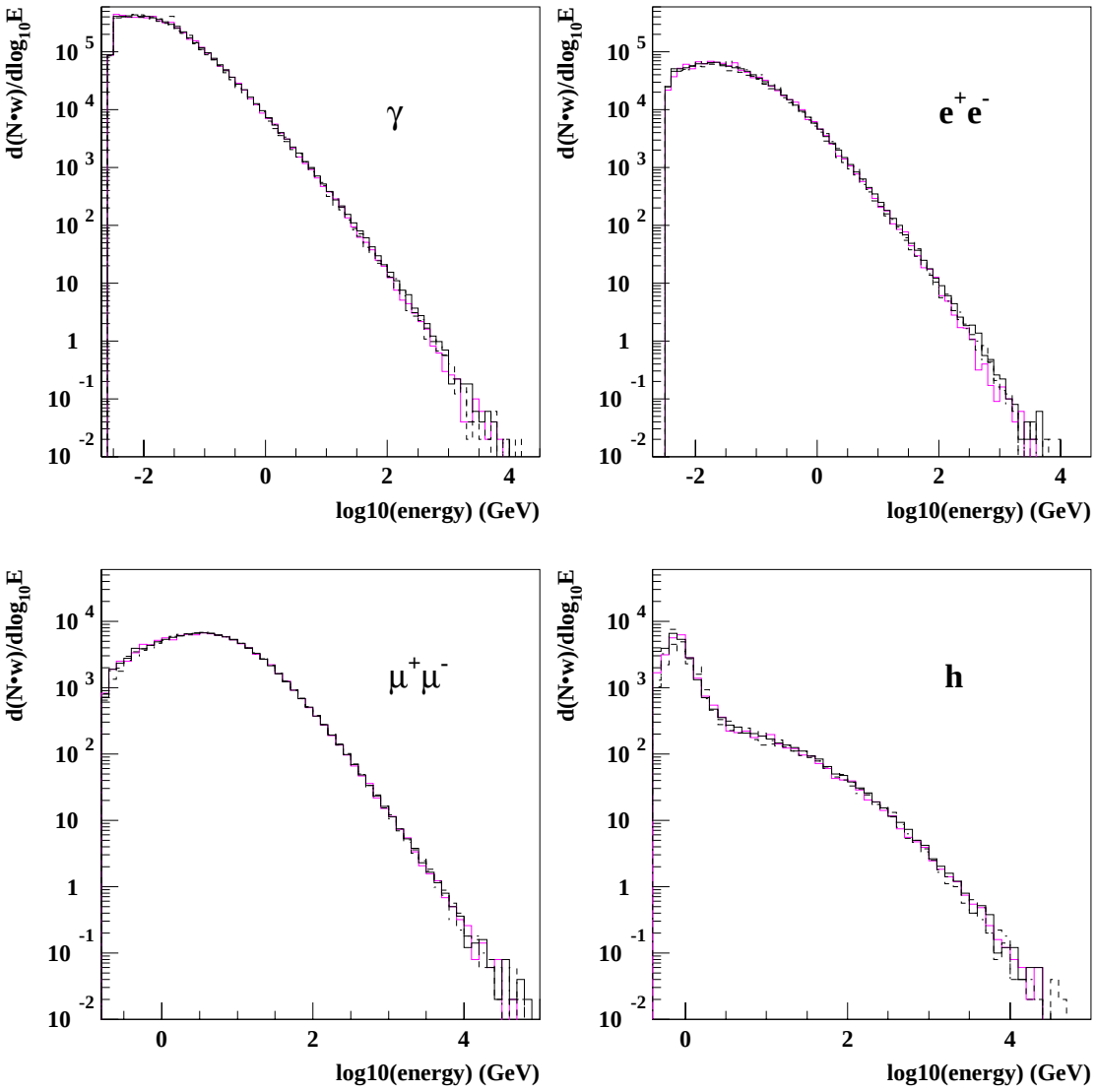

Figure 7: Weighted energy spectra resulting from various stages of thin sampling. The good coincidence of thin sampled spectra in all stages of development with spectra without thin sampling is obvious. Parameters as in Fig. 6.

A special form of case b) occurs mainly in the electromagnetic cascade, where only two particles emerge from an interaction which is shown in Fig. 5c). Here the incoming particle carries an energy $E > E_{thin}$ while both secondaries fall below the threshold E_{thin}. Again one particle is kept, while the chance p_j for retaining also the other secondary j is given by

$$p_j = \sum_i p_i - 1 = \frac{\sum_i E_i}{E_{thin}} - 1 > 0 \quad \text{as} \quad \sum_i E_i > E_{thin} \quad .$$

An additional variant of case b) is shown in Fig. 5d) frequently occurring in brems-

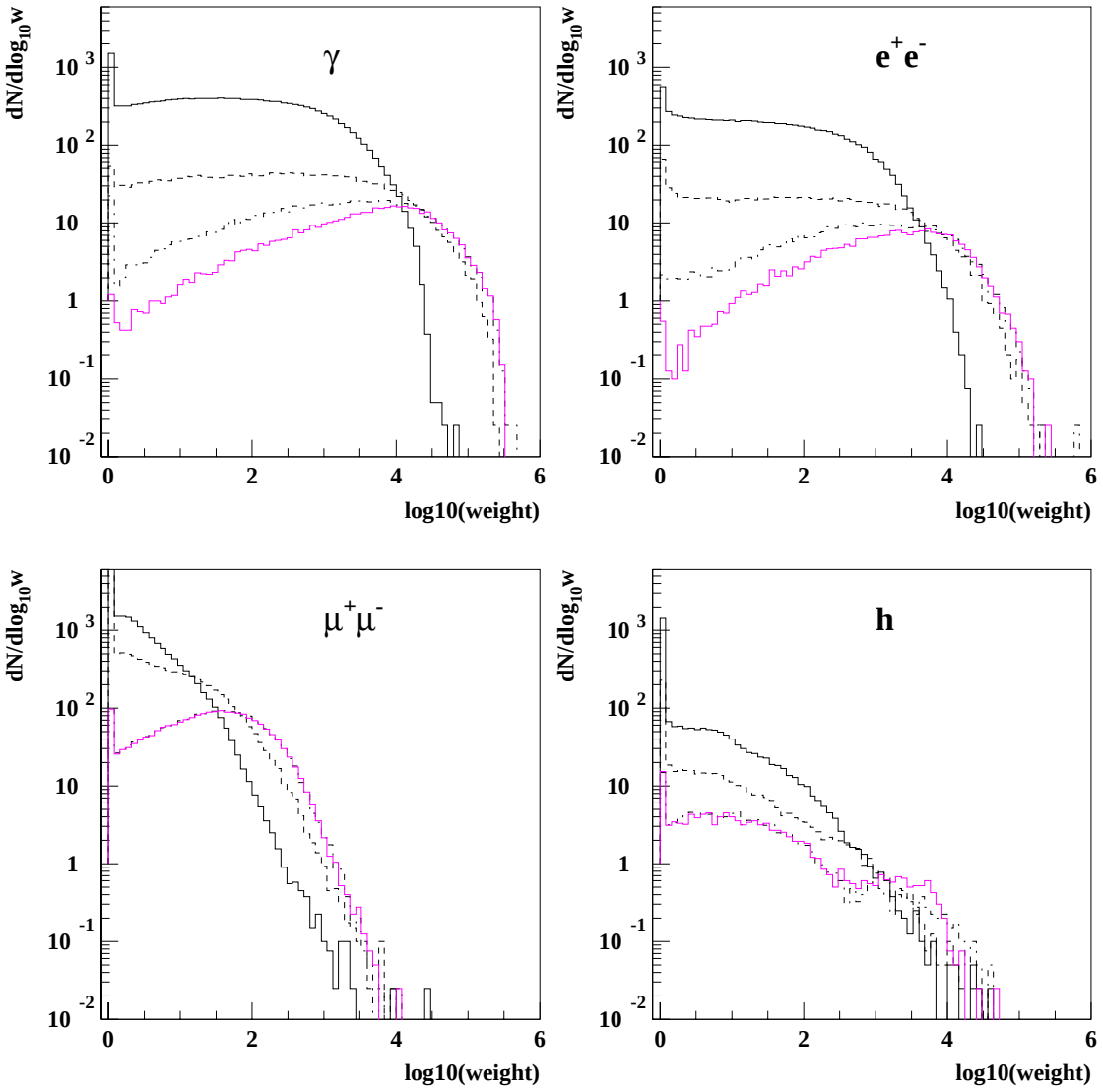

Figure 8: Distribution of particle weights resulting from various stages of thin sampling. Parameters as in Fig. 6.

strahlung processes. The electron or positron keeps the dominant portion of the incoming energy $E > E_{thin}$, while a low energy photon is radiated off. The chance p to retain the photon is given by its energy E_{ph} relative to the thinning level energy

$$p = E_{ph}/E_{thin} \quad .$$

All these cases a) to d) have been realized successively within CORSIKA, each contributing to the improvement of the simulation speed. In the following the results gained with the higher development stages always comprise the use of the earlier development stages, i.e. stage d) comprises stages a) to c).

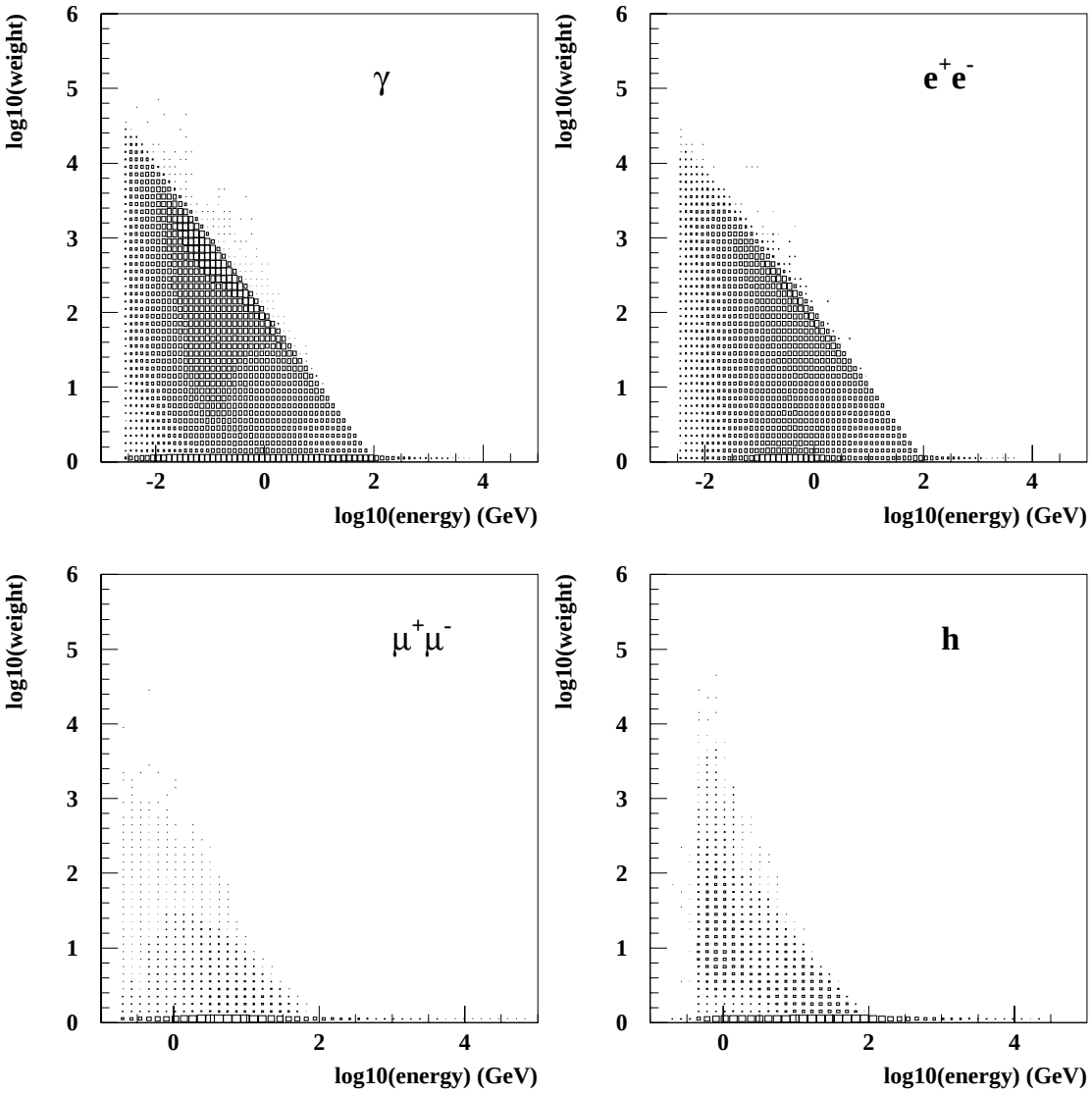

Figure 9: Two dimensional histogram of energy and weight of different particle species after thin sampling with stage a). Parameters as in Fig. 6.

In Fig. 6 the energy spectra of particles arriving at the detector level (110 m a.s.l.) are plotted for different particle species separately, each arriving particle counted once. The spectra without thin sampling are the dotted ones on top of each plot. The reduction in all particle species proceeds with the cumulative activation of stages a) to d). The effectiveness of stage d) on the electromagnetic particles without significant influence onto muonic and hadronic spectra is obvious. If the energy spectra are formed respecting the particle weights the spectra coincide well with spectra without thin sampling, as is demonstrated in Fig. 7.

The distribution of particle weights is shown in Fig. 8. With increasing improvement

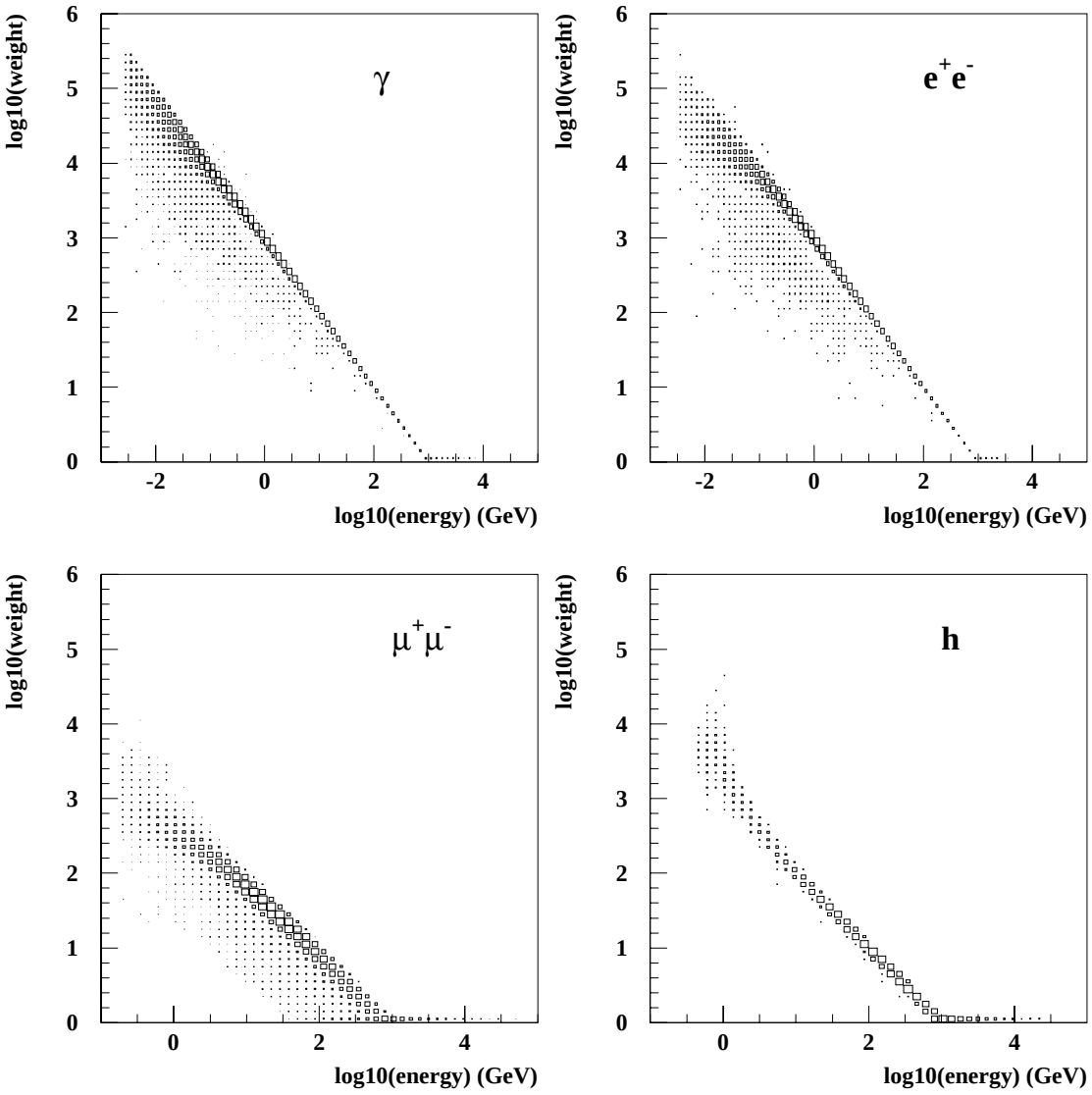

Figure 10: Two dimensional histogram of energy and weight of different particle species after thin sampling including stages a) to d). Parameters as in Fig. 6.

of thin sampling the number of particles with low weight is reduced. The occurrence of weight $w = 1$, as is carried by particles which did not undergo thin sampling, is caused by high energy particles with $E > E_{thin}$ penetrating down to the detector level. This is observed especially for muons and hadrons.

The scatter plots Figs. 9 and 10 show how by the stages of improvement the number of low energy particles with low weight (lower left corner of each plot) is reduced and only the particles along the line $w \cdot E = const$ survive the optimized thin sampling procedure. In Fig. 10 still some few electromagnetic and muonic particles in the low energy range fall below this line. These particles originate from weak interaction

	without thin sampling	thin sampled below 10^3 GeV a)	b)	c)	d)
CPU-time[1]	$\approx 8\ h$	5'44"	1'20"	31"	18"
particles	550960	8136	2187	357	323

[1] for DEC 3000/600 AXP (175 MHz)

Table 1: Effects of various stages a) to d) of thin sampling. The numbers are determined for proton primaries of 10^6 GeV at vertical incidence, QGSJET interaction model, and CORSIKA default parameters.

decays with emission of an unobservable neutrino. In these decays the energy sum of outgoing (observable) particles differs from the incoming energy, which results in a lack of energy for a fixed weight. Therefore this effect does not happen for hadrons. The deviation from the straight line in the low energy tail of the hadronic particles visible in Fig. 10 results from the rest mass included into the energy used in the formulas to calculate the weight of surviving particles.
The gain in computing time and reduced storage requirements for the different stages a) to d) of thin sampling development is summarized in Table 1. Besides the different stages also the thin sampling level influences the required storage for particles and the required CPU-time as is discussed below.

6 Influence of Thin Sampling Level

Of great importance is the energy level below which thin sampling becomes active. Generally with decreasing thin sampling level the CPU-time is increasing and also the number of particles reaching the detector. This is demonstrated with proton induced EAS of 10^{19} eV primary energy in Fig. 11 for the two development stages a) and d). But the gain in CPU-time and the reduced storage requirement with increasing thin sampling level is paied for by an increasing uncertainty in interesting *observable* quantities. This uncertainty is caused by the additional statistical fluctuations which stem from the thin sampling process. The dependence of the uncertainty on the thin sampling level is shown in Fig. 12 for the number of muons arriving at the detector level.
As an example we compare in Fig. 12 the thin sampling levels of different development stages which lead to the same uncertainty of muon number: To reach $\Delta\mu/\mu \leq 0.03$ a thin sampling level of $\varepsilon_{thin} \approx 10^{-4}$ must be used for stage a) and $\varepsilon_{thin} \approx 4 \cdot 10^{-5}$ for stage d). From Fig. 11 we derive for these thin sampling levels CPU-times of $\approx$ 3000 sec for stage a) and only $\approx$ 1000 sec for stage d). A similar behaviour is

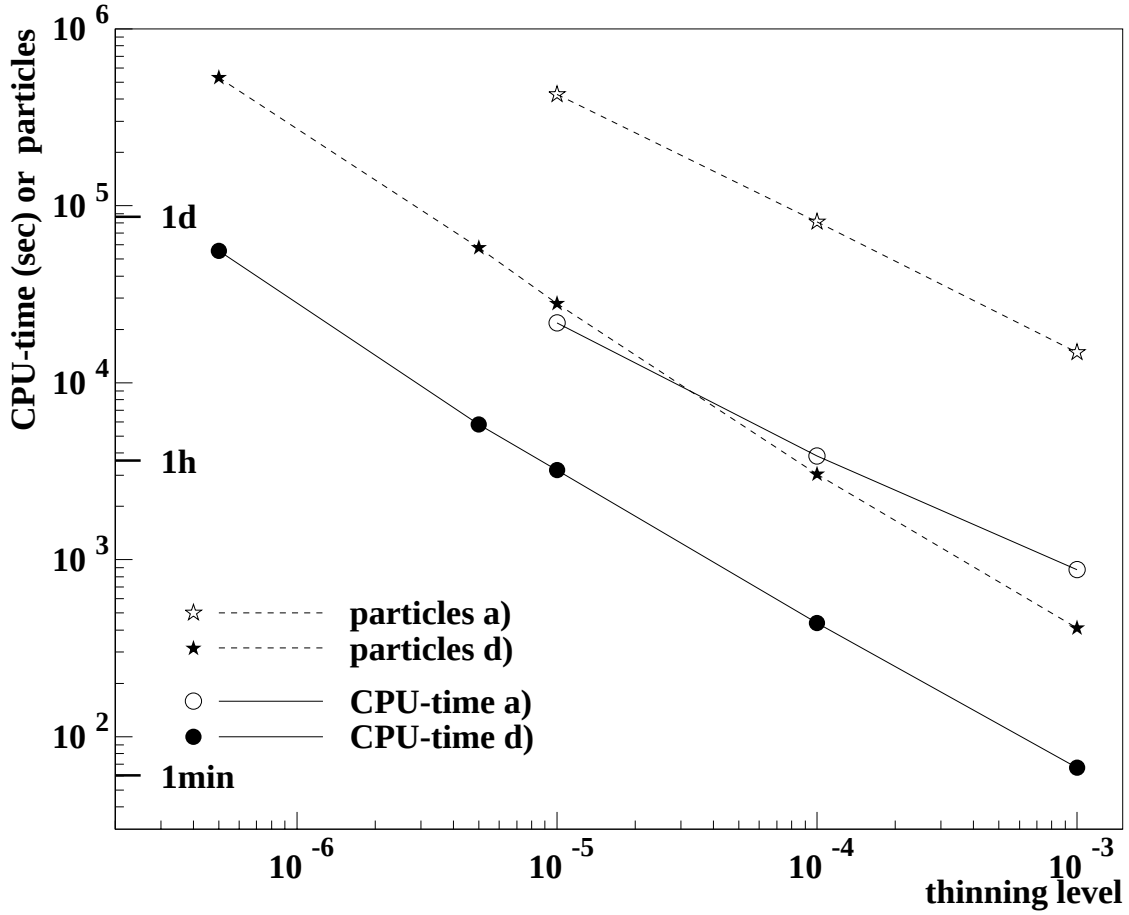

Figure 11: Effect of varying thin sampling level on number of particles arriving at detector level and on CPU-time. The values are established for proton primaries of $E_0 = 10^{19}\ eV$ at vertical incidence using QGSJET interaction model and CORSIKA default parameters. The lines connect the points obtained for development stages a) (open symbols) and d) (filled symbols).

observed for other observable quantities. It demonstrates that with increasing development state the simulation becomes more effective, i.e. for comparable uncertainties much less computing time is needed.

For comparable computing times the uncertainty of measurable quantities is reduced with increasing development stage. For example we consider a CPU-time of 400 *sec* for $\varepsilon_{thin} \approx 10^{-3}$ in stage a) and $\varepsilon_{thin} \approx 10^{-4}$ in stage d), see Fig. 11. In stage a) a value of $\Delta\mu/\mu \approx 0.052$ is reached, while in stage b) the smaller value of $\Delta\mu/\mu \approx 0.04$ is attained, as shown in Fig. 12. This finding justifies the effort put into the various stages of development.

If the thin sampling level is reduced to $\varepsilon_{thin} \approx 10^{-7}$, the additional fluctuations resulting from the thin sampling process become small enough to be dominated by fluctuations anyway inherent in the statistical processes of the EAS development and

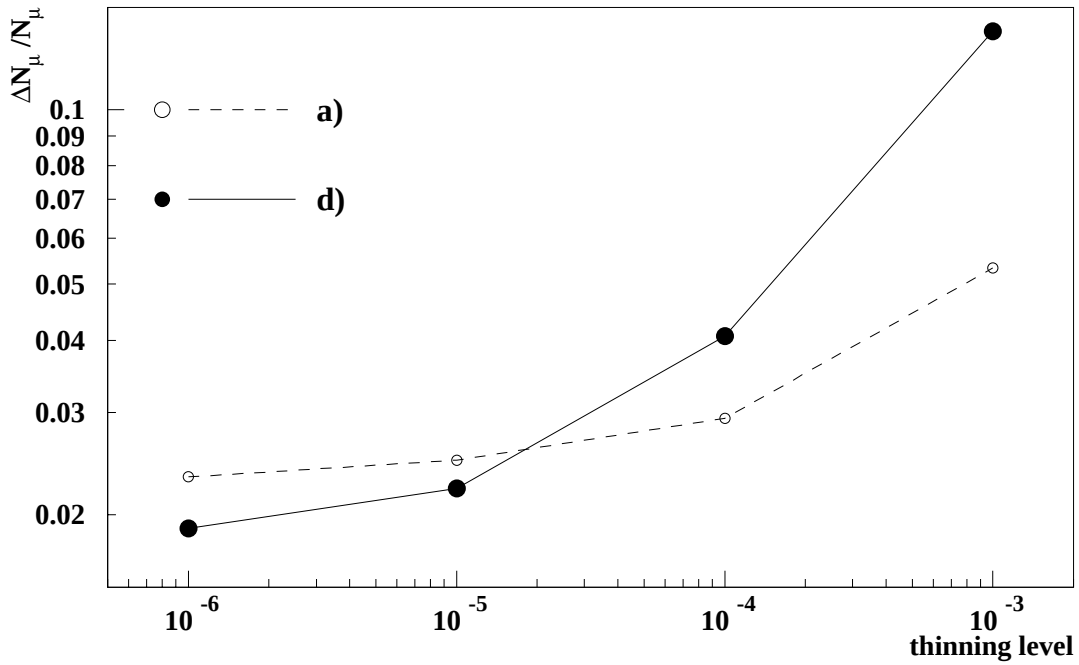

Figure 12: Effect of varying thin sampling level on relative variance of muon numbers (arbitrary units) from proton induced EAS of 10^{19} eV primary energy and vertical incidence using QGSJET interaction model and CORSIKA default parameters. The lines connect points obtained for development stages a) (open circles) and d) (filled dots). Stage d) comprises also stages a) to c). With decreasing thin sampling level the uncertainties caused by thin sampling become smaller and reach the fluctuations inherent in the Monte Carlo simulation at $\varepsilon_{thin} \leq 10^{-7}$.

always present even without application of the thin sampling technique. A further reduction of the thinning level below $\varepsilon_{thin} < 10^{-7}$ brings only marginal improvements in the statistical uncertainties, but needs increasing CPU-times and storage for particles.

7 Conclusions

This work shows that it is possible to simulate EAS also at the highest energies $E_0 > 10^{20}$ eV with the upgraded CORSIKA version 5.60. By the thin sampling procedure the computing times may drastically be reduced to manageable durations but on the expenses of increased statistical fluctuations. The optimum choice of the thin sampling level depends on the needs and constraints of the individual problem to be studied.

Acknowledgements

We are indebted to C. Pryke (Chicago, USA) who stimulated the improvements of CORSIKA by many e-mail discussions. Our thanks go also to S. Sciutto (La Plata, Argentina), who brought our attention to the LPM-suppression routines of MOCCA and AIRES.

References

[1] N. Chiba et al., *Nucl. Instr. Meth.* **A311** (1992) 338; N. Hayashida et al., *J. Phys. G: Nucl. Part. Phys.* **21** (1995) 1101

[2] D.J. Bird et al., *Nucl. Instr. Meth.* **A349** (1994) 592; D.J. Bird et al., *Ap. J.* **441** (1995) 144

[3] N.N. Kalmykov, G.B. Khristiansen, *J. Phys. G: Nucl. Part. Phys.* **21** (1995) 1279; B.N. Afanasiev et al., *Proc. 25rd Int. Cosmic Ray Conference*, Durban, **6** (1997) 229

[4] Auger Collaboration, Pierre Auger Project Design Report, Fermilab (1997)

[5] D. Heck et al., Report **FZKA 6019** (1998), Forschungszentrum Karlsruhe

[6] J. Ranft, *Phys. Rev.* **D51** (1995) 64

[7] J.N. Capdevielle et al., Report **KfK 4998** (1992), Kernforschungszentrum Karlsruhe

[8] N.N. Kalmykov, S.S. Ostapchenko, *Yad. Fiz.* **56** (1993) 105; *Phys. At. Nucl.* **56**(3) (1993) 346; N.N. Kalmykov, S.S. Ostapchenko and A.I. Pavlov, *Bull. Russ. Acad. Sci. (Physics)* **58** (1994) 1966

[9] R.S. Fletcher, T.K. Gaisser, P. Lipari and T. Stanev, *Phys. Rev.* **D50** (1994) 5710; J. Engel, T.K. Gaisser, P. Lipari and T. Stanev, *Phys. Rev.* **D46** (1992) 5013

[10] K. Werner, *Phys. Rep.* **232** (1993) 87

[11] J. Knapp, D. Heck and G. Schatz, Report **FZKA 5828** (1996), Forschungszentrum Karlsruhe

[12] J. Knapp, Report **FZKA 5970** (1997), Forschungszentrum Karlsruhe

[13] J. Knapp et al., to be published

[14] H.H. Mielke et al., *J. Phys. G: Nucl. Part. Phys.* **20** (1994) 637

[15] G.B. Yodh et al., *Phys. Rev.* **D27** (1983) 1183

[16] T.K. Gaisser et al., *Phys. Rev.* **D36** (1987) 13503

[17] R.M. Baltrusaitis et al., *Phys. Rev. Lett.* **52** (1993) 1380

[18] M. Honda et al., *Phys. Rev. Lett.* **70** (1993) 525

[19] L.D. Landau and I.Ya. Pomeranchuk, *Dokl. Akad. Nauk SSSR* **92** (1953) 535 & 735

[20] A.B. Migdal, *Phys. Rev.* **103** (1956) 1811

[21] S. Sciutto, private communication (1997)

[22] A.M. Hillas, *Proc. 17th Int. Cosmic Ray Conference*, Paris, **8** (1981) 193

[23] E. Konishi et al., *J. Phys. G: Part. Phys.* **17** (1991) 719

[24] A.M. Hillas, *Nucl. Phys. B (Proc. Suppl.)* **52B** (1997) 29

[25] W.R. Nelson, H. Hirayama and D.W.O. Rogers, Report **SLAC 265** (1985), Stanford Linear Accelerator Center

[26] J. Knapp and D. Heck, Report **KfK 5196B** (1993), Kernforschungszentrum Karlsruhe; for an up–to–date version see http://www-ik3.fzk.de/~heck/corsika